RESEARCH ON REGIONAL PREDICTABILITY AT KNMI

Jan Barkmeijer, Robert Mureau, Jeroen Oortwijn and Theo Opsteegh
Royal Netherlands Meteorological Institute
PO BOX 201, 3730 AE De Bilt, The Netherlands.

Abstract

In the first part of this paper the KNMI ensemble prediction system (KEPS) is presented. The method is based on the assumption of linear error growth. It uses adjoint models and is applied for the short term only.

In the second part the sensitivity of the onset of two weather regimes with respect to initial conditions is studied. The weather regimes are a Euro-Atlantic blocking regime and a Euro-Atlantic strong zonal flow regime. Perturbations are computed which trigger the onset of a weather regime in the linear range as well as in the nonlinear range. It is shown that moderate initial perturbations occasionally trigger a transition from a blocking regime to a zonal flow regime, or vice versa, within three days. For an optimization time of six days, the iteratively computed perturbations generate such transitions for almost all investigated cases.

1 Introduction

One of the intriguing aspects of present weather forecasting is the variability in the quality of the forecasts. Sometimes a forecast is accurate for up to a week but it also occurs that a forecast has lost skill after a few days. Part of the variability in skill can be explained as a statistical effect. This is because the initial error partly results from random observational errors. The forecast error will therefore have a random component. Thus one particular forecast must be considered as an arbitrary member of a probability distribution.

Lorenz (1965) proposed the Monte Carlo method for studying the quality of forecasts. A small ensemble of randomly chosen initial states is integrated with the forecast model. The spread between the ensemble members is considered as a measure of the atmospheric predictability. However, the complexity of the current forecast models greatly obstructs the operational use of the Monte Carlo method. A more fundamental problem is how to obtain a good statistical description of the initial errors. Such a description is necessary for selecting a representative sample. All current skill prediction methods suffer from the lack of knowledge on the statistics of the initial error.

A major development in meteorology was the introduction of adjoint models (Marchuk 1974). The great advantage of adjoint models is that one can

easily compute gradients of multi-variable functions. In predictability research this property is employed to study error growth in an efficient manner (Errico and Vukicevic 1992, Barkmeijer 1992) by determining the sensitivity of one aspect of the forecast, such as local pressure, to uncertainties in the initial conditions. With an adjoint model, it is possible to retrieve this sensitivity pattern in the initial conditions by integrating the adjoint model only once backwards in time. Thus, it is not necessary to integrate the forecast model with a perturbation once for each coordinate in order to obtain the impact of an arbitrary initial perturbation. From this, it is clear that adjoint models are useful in computing the patterns that give the maximal forecast error in a certain area at a pre-chosen forecast time. These sensitivity patterns are usually referred to as singular vectors (Farrell 1989, Zhang 1988). At a fixed forecast time, they show a larger error growth than the exponentially growing normal modes. Molteni and Palmer (1993) and Mureau et al (1993) employ singular vectors for ensemble forecasting.

A basic assumption in using adjoint models is that the error dynamics is linear. Studies by Vukicevic (1991) and Errico et al(1993) indicate that this is the case for forecast periods up to 72 hours. In Barkmeijer and Opsteegh (1992) a predictor for regional forecast skill is suggested which can benefit from the use of adjoint models. The predictor of the skill is the maximum likely amplitude of the squared error in the streamfunction field at 500 hPa for a pre-chosen area and forecast period. It is given by the largest value of the covariance matrix of the local forecast error. Results indicate that the predictor gives significant information about the quality of the local forecast.

This work has led to the introduction of an ensemble prediction system in the operational division of the Netherlands Weather Institute. The method is based on the assumption of linear error growth. It uses adjoint models and is applied for the short term only. In the first part of this paper we will describe the KNMI ensemble prediction system (KEPS).

In the second part we will discuss the predictability of weather regime transitions. In spite of the atmosphere's limited predictability the atmospheric circulation still exhibits some regular behaviour, even for periods longer than 2 weeks. In the extra-tropics, persistent large-scale atmospheric flow patterns are observed. The low-frequency variability of the extra-tropical atmosphere can be considered to be mainly due to the alternation between several of such weather regimes, interrupted by transition periods (Vautard 1990). The maintenance of weather regimes is fairly well investigated. On the other hand, the onsets and breakdowns of weather regimes are still poorly understood. In this paper, we study the potential for the excitation of a weather regime or a weather regime transition by adding small perturbations to the initial conditions which are optimal in some prescribed sense. We consider only two regimes. The first regime is the Euro-Atlantic blocking regime. The second one is a strong zonal flow regime in the same geographical area. In the latter,

the weather is highly variable because of the continuous advection of weather systems.

In section 2 the KNMI ensemble prediction system KEPS is described. In section 3 we outline the characterization of regimes. In section 4 we derive a method to compute initial perturbations that are optimal in triggering regime transitions. Results for the quasi-linear range are presented in section 5. In section 6 a modification of the method is presented which enables extension of the method into the nonlinear range. Results of the modification method are presented in this section. Finally some concluding remarks are given in section 7.

2 KNMI ensemble prediction system (KEPS)

2.1 Generation of the ensemble

For the generation of the ensemble we use a 3-level quasi-geostrophic model triangularly truncated at wavenumber 42, the tangent linear model and its adjoint. For a description of the model we refer to Marshall and Molteni (1993). We will denote this model by T42QG. The numerical costs of running these models are low. The contribution of model errors to the forecast error is not included in KEPS. As a further simplification we assume that the error dynamics is linear. The integration of an initial error $\epsilon(0)$ to time T of the forecast is done with the tangent linear T42QG model. This gives rise to a linear operator R(0,T) such that:

$$\epsilon(T) = R(0,T)\epsilon(0) \tag{1}$$

For convenience we leave from now on the time dependence of R from the notation. We point out that R has to be determined each day because it depends on the daily varying reference orbit. The reference orbit used in the KEPS integration is derived from the operational forecast of the ECMWF model.

We assume that we have no knowledge of the initial error distribution. For the initial error covariance matrix we take the identity matrix and assume that the errors are normally distributed. This means that the errors in the different spectral modes are initially uncorrelated. Their squared amplitudes have the same expectation value.

Apart from using a time-independent covariance matrix for the initial error, the computational costs can be reduced still further, by performing skill forecasts for a restricted area . We are interested in the quality of forecasts in a restricted area over Europe at 500 hPa (see Fig. 2). We reduce the dimension

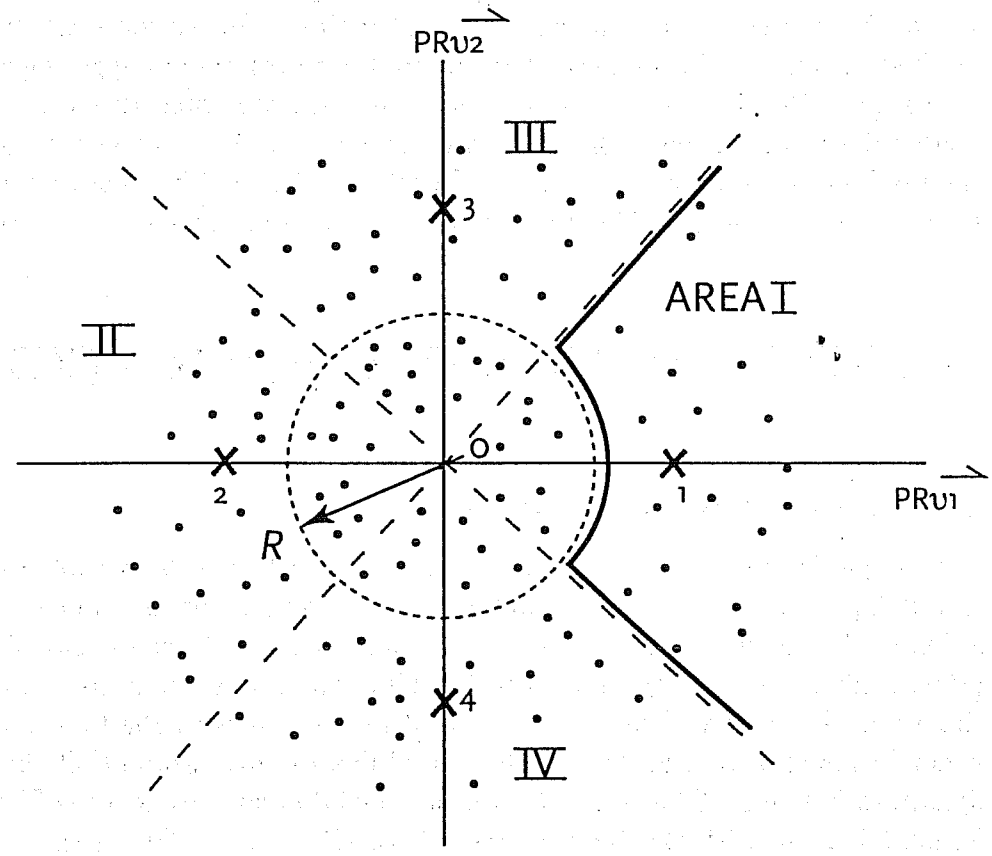

Fig. 1. Illustration of the clustering. The horizontal axis is the amplitude of the integrated regional singular vector 1 and the vertical axis is the same for vector 2. The dots are the ensemble members. The radius R of the circle is the climatalogical error in geopotential height at 500 hPa of the ECMWF model for the region indicated in Figure 2. The origin is the operational forecast, it is defined as cluster zero. All ensemble members within the circle are part of cluster zero. The other clusters are indicated with 1 to 4. Their amplitude and probabilities are computed from the ensemble members within their domain of influence.

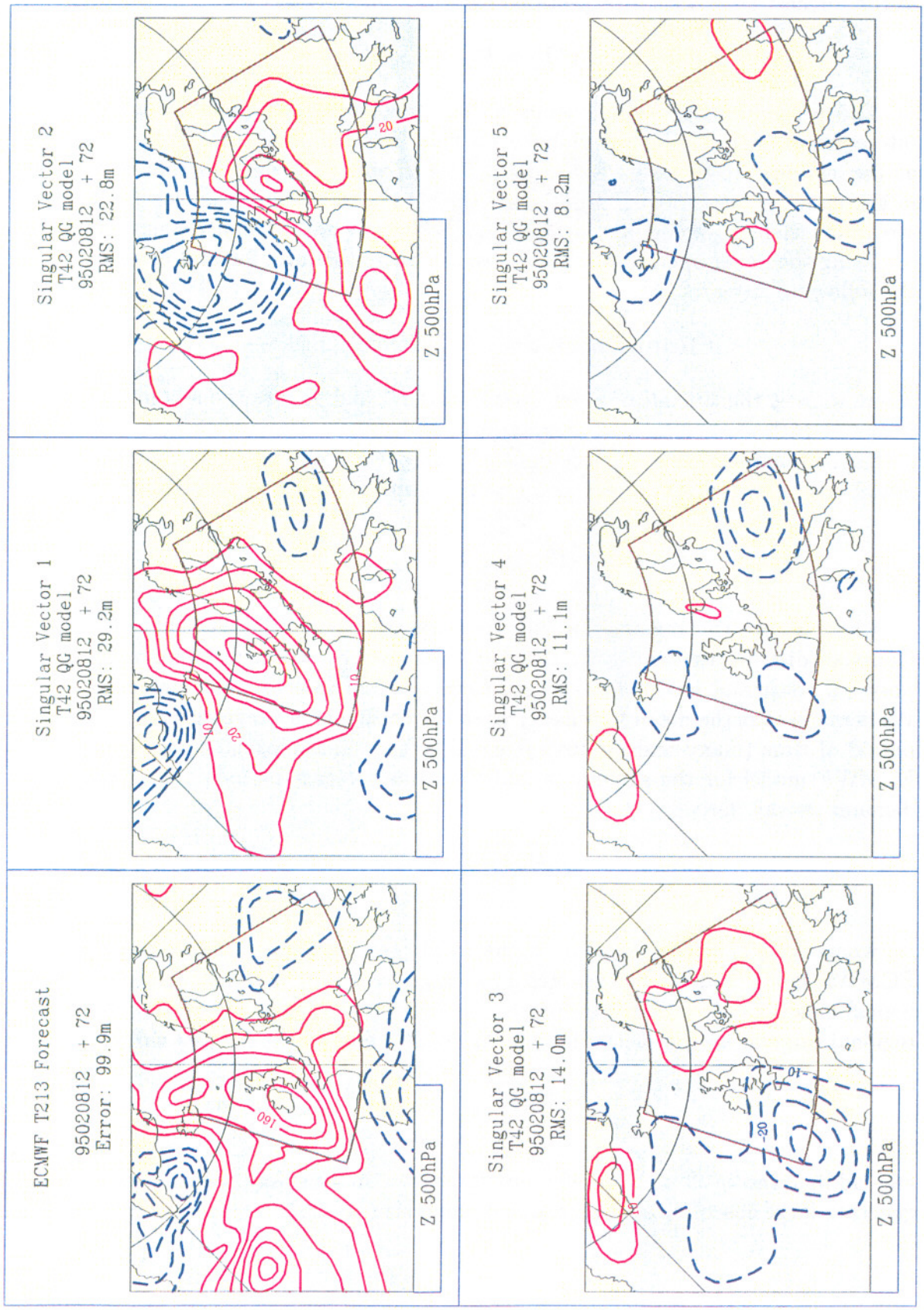

Fig. 2. The error in geopotential height at 500 hPa over Europe in three day forecast of the ECMWF model for 950211 and the first five regional singular vectors integrated of the time of forecast. The singular vectors are computed for the area as indicated in the figure.

of the forecast error with a projection operator P defined by:

$$\eta(T) = P\epsilon(T) \tag{2}$$

The projection operator depends on the meteorological quantity one is interested in. Here $\epsilon(T)$ is the global error field in streamfunction coordinates at the various model levels for forecast time T and $\eta(T)$ denotes the error in geopotential height at 500 hPa in the restricted area. The conversion from streamfunction to geopotential height is done with the linear balance equation.

Using the linear operators R and P, we can write the local forecast error in the following form:

$$< PR\epsilon(0), PR\epsilon(0) >=< R^*P^*PR\epsilon(0), \epsilon(0) > \tag{3}$$

where $<,>$ is the Euclidean innerproduct and P^* and R^* are the adjoints of P and R with respect to this inner product. The eigenvalues λ^2 of R^*P^*PR correspond with regional eigenvectors ν. Making use of our assumption on the initial error distribution we can generate an ensemble of initial perturbations:

$$\epsilon(0) = \sum_{i=1}^{n} a_i \nu_i \tag{4}$$

where ν_i are the regional singular vectors and a_i are the elements of a Gaussian distribution with zero mean and variance σ. We determined σ by posing a constraint on the local forecast error size of the ensemble members. We demand that the mean forecast error of the ensemble, averaged over a long period of time (many realisations), is equal to the climatological error of the ECMWF model for the same area and the same forecast period. From this demand we can derive:

$$\sigma = \frac{< \overline{\eta(t), \eta(T)} >_{ECMWF}}{\sum_{i=1}^{n} \overline{\lambda_i^2}} \tag{5}$$

where $< \overline{\eta(t), \eta(T)} >_{ECMWF}$ is the local forecast error variance of the ECMWF model and the bar denotes an average over many forecasts (climatological mean). The ensemble of forecasts is now computed by integrating the regional singular vectors with the tangent linear model to the forecast time T:

$$\eta(T) = \sum_{i=1}^{n} a_i PR\nu_i \tag{6}$$

and adding the $\eta(T)$ to the reference forecast. In this way we can easily generate large ensembles. We use an ensemble size of 2000.

2.2 Clustering

In practice we only use the first two regional singular vectors in the computation of the ensemble. Their eigenvalues are usually much larger than the subsequent eigenvalues. The information is clustered into five patterns as follows (see Fig. 1). The first cluster is the operational forecast (cluster 0). Its probability is determined by the number of ensemble members that deviate less from the operational forecast than the climatological mean regional error of the ECMWF model for the considered forecast period. The remaining four clusters are determined by adding and subtracting the forecasted singular vectors 1 and 2 to the reference forecast. Their amplitude is determined by the mean amplitude of the ensemble members that are located in the influence area of those four clusters. The probability of occurrence is determined by the number of ensemble members in each of the clusters. Because of the linearity of the approach and the definition of the clusters the probability for clusters 1 and 2 should be the same as well as 3 and 4. Small differences are due to sampling errors.

2.3 Example of an ensemble forecast

As an example of KEPS we show the ensemble forecast from Wednesday 8 February 1995 for Saterday 11 February. Figure 2 displays the forecast error in geopotential height at 500 hPa of the ECMWF model and the first five singular vectors which are integrated to the time of the forecast with the tangent linear model. It is clear that the error in this case projects strongly on the first singular vector.The amount of detail in the T42QG singular vectors seems adequate to describe the detailed structure of the forecast error of the ECMWF model. Figure 3 displays the computed clusters of KEPS. Cluster 0 is the operational forecast. Its probability is 42%. This is quite low, usually it is 80% or higher. So the forecaster should be alerted by this figure. The alternative clusters (called scenarios in the figure) have probabilities, that are lower than the operational forecast but are not insignificant. The verifying analysis, displayed in the lower left corner, shows that scenario 2 is the best forecast. Its RMS error is 58.5 m whereas the RMS error of the operational forecast is 99.9 m. In reality the ridge that was predicted over the UK was weaker and had progressed a little bit farther east. This information on the uncertainty in strength and position of synoptic scale waves is very important for the prediction of the intensity and timing of weather events. This is illustrated by the coloured areas. They show the estimated position of the frontal systems in the various scenarios. We have computed this from a crude estimate of the vertical motion field (we have assumed that the vertical motion is proportional to the relative vorticity advection only, so we have neglected the temperature advection here. This will be improved in the near future). The scenarios in-

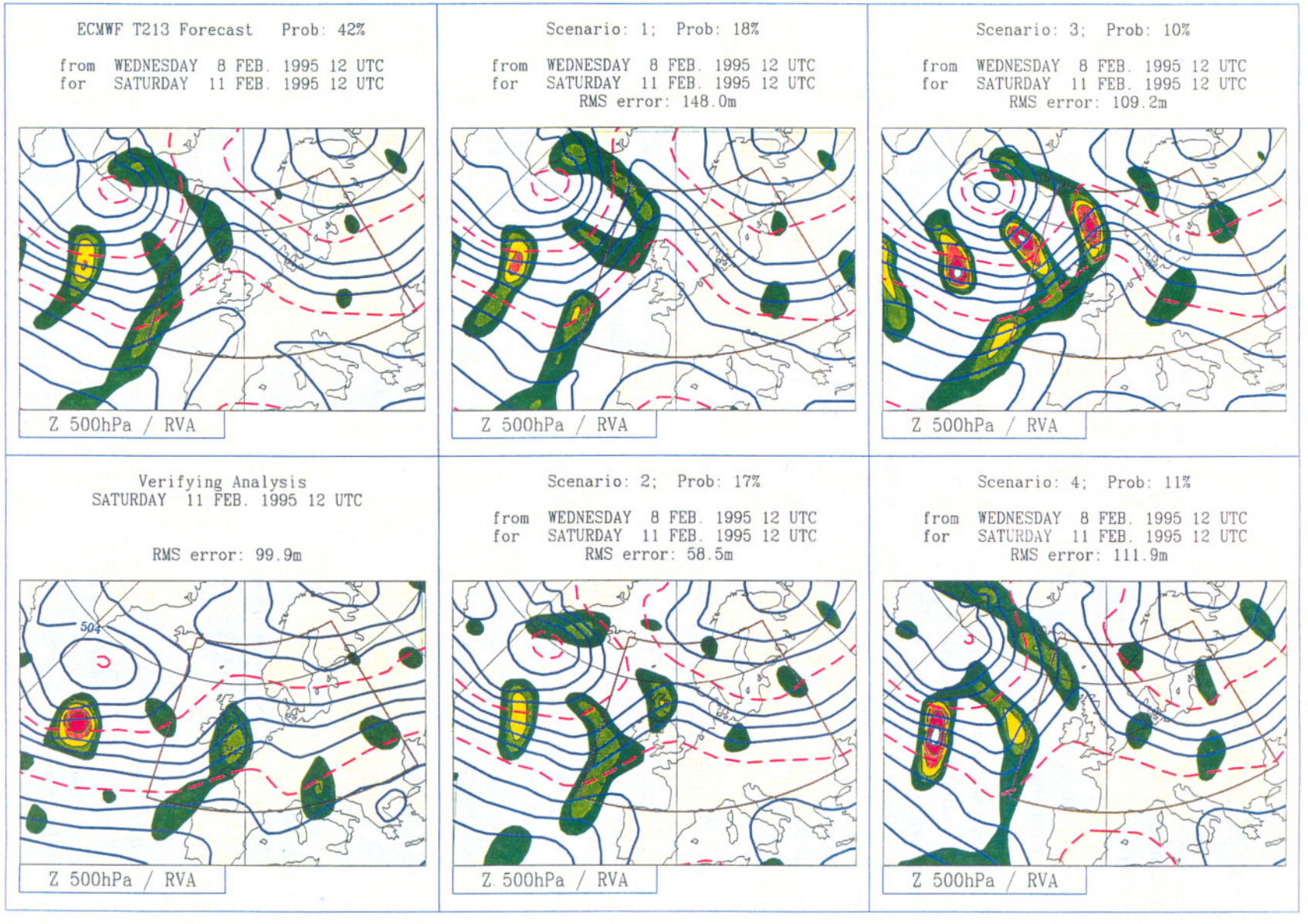

Fig. 3. The upper left corner displays the operational three day forecast at 500 hPa over Europe of the ECMWF model for 950211 (cluster zero). In the lower left corner is the verifying analysis. Ythe other figures are the alternative cluster or scenarios. The computed probabilities and the verifying RMS errors are indicated for each of the scenarios. The coloured areas are estimates of the position of the frontal systems.

dicate clearly the uncertainty in strength and position of the frontal system over the UK. The operational forecasters at KNMI are beginning to use this information on a regular basis. As we are computing probabilities of small errors in the short term forecast of the ECMWF model we will concentrate on variables which clearly display small amplitude and phase errors. We are doing this by dealing with the vertical motion field and other frontal parameters.

3 Characterization of weather regimes

Many different criteria have been used to characterize an atmospheric blocking regime. The best known criteria are those by Rex (1950a,b) and Dole (1978). In this paper we focus on the atmospheric flow over Europe. Using observations for 10 winter seasons (DJF) from 1982/83 to 1991/92, Liu (1994) found that a Euro-Atlantic blocking regime can be characterized by a dipole-like pattern, consisting of a very strong positive geopotential height anomaly with its center at about 60^0 N and a weaker negative anomaly south of it. Furthermore, he found that a strong zonal flow regime is characterized by the opposite dipole pattern. So, both regimes have approximately the same anomaly pattern with respect to the climatological mean but with opposite sign. Liu computed this anomaly pattern, which he called the blocking geopotential height anomaly pattern z_b, for the 10 winter season dataset and for a dataset simulated by a T21QG model (Liu and Opsteegh 1994). The latter z_b pattern is the mean 500 hPa geopotential height anomaly pattern for the 10000 days out of 45000 days of integration which had the largest positive anomalies at 60^0 N. This pattern is shown in Fig. 4. It is very similar to the pattern computed for the observed winter season dataset. Based on these results Liu (1994) and Liu and Opsteegh (1994) defined a single index which measures the resemblance of a particular circulation pattern with the blocking regime or the strong zonal flow regime. This index is called the blocking index $\mathcal{B}$. The blocking index $\mathcal{B}$ for a particular circulation pattern is defined by the projection of the daily geopotential height anomaly pattern z_d on the blocking geopotential height anomaly pattern z_b, weighted with the norm of z_b. The blocking index $\mathcal{B}$ of a certain flow pattern with stream function ψ is given by

$$\mathcal{B}(\psi) = \frac{< z_d(\psi), z_b >}{< z_b, z_b >} , \tag{7}$$

where the brackets denote a squared norm inner product on a sphere, integrated over height

$$< x, y >= \frac{1}{4\pi} \int\int\int x\ y\ dV. \tag{8}$$

The relation between z_d and ψ is given by

$$z_d(\psi) = L_z\psi - z_c , \tag{9}$$

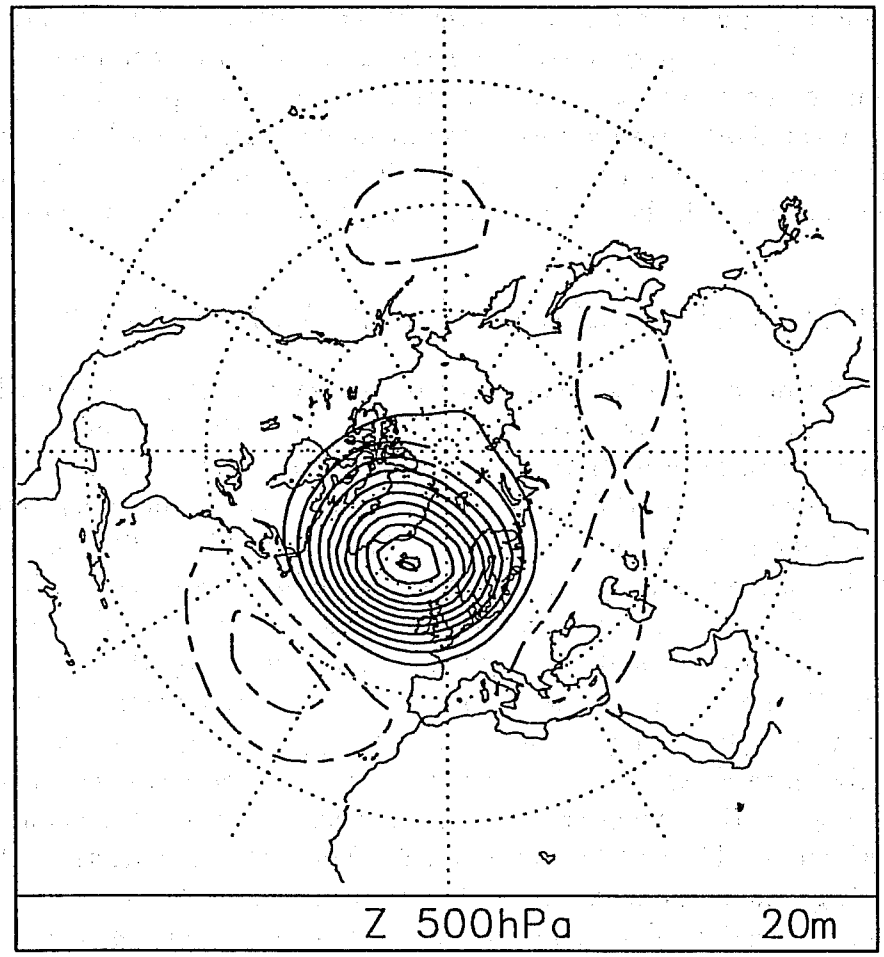

Fig. 4. Blocking anomaly pattern: mean 500 hPa geopotential height anomaly pattern for the 10000 days out of 45000 days with the largest positive anomalies at 60^0 N. The contour interval is 20 m. Solid lines correspond to positive values, dotted lines to negative values.

where L_z is the linear operator which transforms streamfunction into geopotential height and z_c is the climatological mean geopotential height. The geopotential height field is obtained from the streamfunction by solving the linear balance equation. A circulation pattern with $\mathcal{B} > 0.5$ ($\mathcal{B} < -0.5$) can be considered as a blocked flow (strong zonal flow). Furthermore, the larger $\mathcal{B}$ the more pronounced the blocked flow is and the more negative the stronger the zonal flow is. Typical values of $\mathcal{B}$ are between -2 and 2.

4 Perturbations triggering a regime onset

The blocking index $\mathcal{B}$ characterizes in a simple manner whether a given atmospheric circulation pattern can be associated with a blocking regime or a strong zonal flow regime. Small perturbations in the initial conditions of a forecast will alter $\mathcal{B}$ at a certain forecast time. It may even occur that $\mathcal{B}$ changes sign, corresponding to a regime transition. We want to investigate how the predicted value of $\mathcal{B}$ depends on small changes in the initial conditions. Therefore, we will determine the initial perturbation which maximizes the difference in $\mathcal{B}$ between the reference forecast and the forecast made from the perturbed initial state at a prescribed forecast time. In other words, this perturbation maximizes the difference between the two forecasts in the direction of phase space corresponding to the dipole-like anomaly pattern. This approach could be considered as an extension of the study of Barkmeijer (1995), where error growth is maximized in a single grid point.

For the computations, we use the 3-level quasi-geostrophic model, but now triangularly truncated at wavenumber 21 (T21QG), its tangent linear and adjoint versions. The evolution of a stream function perturbation is given by the tangent linear operator R, such that

$$\epsilon(T) = R(0,T)\ \epsilon(0)\ . \tag{10}$$

The period for which error growth is linear will be called the linear-range. With realistic analysis errors the evolution of errors is linear up to about 72 hours. However, the length of the linear-range is not constant but depends on the synoptic situation, the model used and the amplitude and structure of the error itself (Lacarra and Talagrand 1988). In this work, we will assume that the T21QG model describes the evolution of the atmospheric flow perfectly, i.e. a perfect model approach. So, all forecast errors are due to errors in the initial conditions.

We are interested in the perturbation ϵ, keeping

$$||\epsilon(0)||^2 =< \epsilon(0), \epsilon(0) > \tag{11}$$

fixed, which maximizes

$$\mathcal{B}(\psi(T) + \epsilon(T)) - \mathcal{B}(\psi(T)) \tag{12}$$

at prescribed forecast time T. Using the definition of $\mathcal{B}$ (7), this can be written as

$$\frac{< L_z(\psi(T) + \epsilon(T)) - z_c, z_b > - < L_z\psi(T) - z_c, z_b >}{< z_b, z_b >} . \tag{13}$$

The denominator is just a constant. Therefore, maximizing (13) is equivalent to maximizing

$$< L_z\epsilon(T), z_b > = < L_z R\epsilon(0), z_b > = < \epsilon(0), R^* L_z^* z_b > , \tag{14}$$

where we introduced the operators R^* and L_z^* which are the adjoint operators of R and L_z, respectively, with respect to the squared norm inner product. A good introduction to the application of adjoint methods in meteorology has been given by Talagrand and Courtier (1987). It follows that the initial perturbation which maximizes the difference in $\mathcal{B}$ at optimization time T is given by

$$\epsilon_L(0) = \lambda R^* L_z^* z_b . \tag{15}$$

The absolute value of the scaling factor λ is fixed through constraint (11). When choosing λ positive, ϵ_L maximizes the change towards a blocking regime. A negative value of λ results in a maximum change towards a strong zonal flow regime. The pattern ϵ_L is related to the sensitvity fields described in Rabier et al. (1993). The difference in $\mathcal{B}$ at optimization time between the reference and perturbed forecast for this optimal perturbation is

$$\Delta\mathcal{B} = \frac{||R^* L_z^* z_b||}{||z_b||^2} \, ||\epsilon_L(0)|| . \tag{16}$$

The difference $\Delta\mathcal{B}$ is a linear function of the length of the optimal perturbation vector, provided the maximization period is kept constant. This linear relation is only valid for small initial perturbations, i.e. in the linear-range.

We now define the linear sensitivity by

$$S_L = \frac{||R^* L_z^* z_b||}{||z_b||^2} . \tag{17}$$

The linear sensitivity S_L is a measure for the (maximum) divergence of trajectories when projected onto the direction of phase space that corresponds to the blocking anomaly pattern. We will see that adding a moderate perturbation $\epsilon_L(0)$, as given in (15), to the reference forecast that has high linear sensitivity S_L for a forecast period of 3 days may already lead to a substantial difference in $\mathcal{B}$. Even a regime transition is sometimes triggered within 3 days.

We want to emphasize that the numerical costs of the computation of $\epsilon_L(0)$ are very low. Only one backward integration of the adjoint model is needed.

5 Results for the quasi-linear range

Starting from an arbitrary initial condition, we integrated T21QG for 1200 days. We computed the blocking index each day for the final 1000 days. A part of the time series obtained in this way is presented in Figs 5a and 5c. The single valued function $\mathcal{B}$ is a very useful quantity to decide whether the model state is in a blocking regime ($\mathcal{B} > 0.5$) or in a strong zonal flow regime ($\mathcal{B} < -0.5$). The T21QG model is capable of entering both regimes in a realistic way (Marshall and Molteni 1993; Liu and Opsteegh 1994). From Figs 5a and 5c it is clear that regime transitions extend over some days but are sometimes very abrupt (e.g. around day 60).

The linear sensitivity S_L for a forecast period of 3 days is computed for the same time series and is given in Figs 5b and 5d. A high linear sensitivity for a certain day d means that $\mathcal{B}$ will differ substantially at day $d+3$ if the optimal perturbation is added to the reference flow at day d. The real difference $\Delta\mathcal{B}$ depends on the amplitude of the initial perturbation and on the degree of linearity of the error growth. Low values of S_L indicate that moderate initial perturbations are not capable of changing the flow substantially towards a blocking or strong zonal flow regime. This indicates a high predictability of the regime type, because no initial perturbation can change the evolution of the flow strongly towards one of the regimes. So, if there is not a regime transition in the forecast, it is likely that the flow remains in the same regime. However, when there is a regime transition forecasted, it is likely that it will occur. In cases of high values of S_L moderate initial perturbations which change the flow towards one of the regimes can be found, so that the predictability is less in this situation. However, the difference $\Delta\mathcal{B}$ due to ϵ_L is an upper bound. So, a low sensitivity to the optimal error $\epsilon_L(0)$ implies a relatively high predictability of the regime type. On the other hand, a high sensitivity to $\epsilon_L(0)$ does not necessarily imply a high sensitivity to a (random) analysis error.

Figures 5b and 5d show that there are days where the sensitivity is small and days where the sensitivity is high. Differences may be as large as a factor of 5. Notice that the periods with a high linear sensitivity are very short. The majority of the days are insensitive to regime transitions.

Considering together Figs 5a and 5b and also Figs 5c and 5d, we see that low sensitivity can go along with quasi-stationary flows (e.g. around day 80) or with situations where a transition takes place (e.g. around day 60), which means that this particular transition is highly predictable. During periods with a high sensitivity, transitions may (e.g. around days 130,730) or may not occur (e.g. around day 690). The same characteristic features can be found in the simple three-variable Lorenz convective model (Lorenz 1963; Palmer 1993).

To illustrate what the impact of ϵ_L is during a period with a high sensitivity we select day 687. The initial optimal perturbation $\epsilon_L(0)$ for the period 687 to

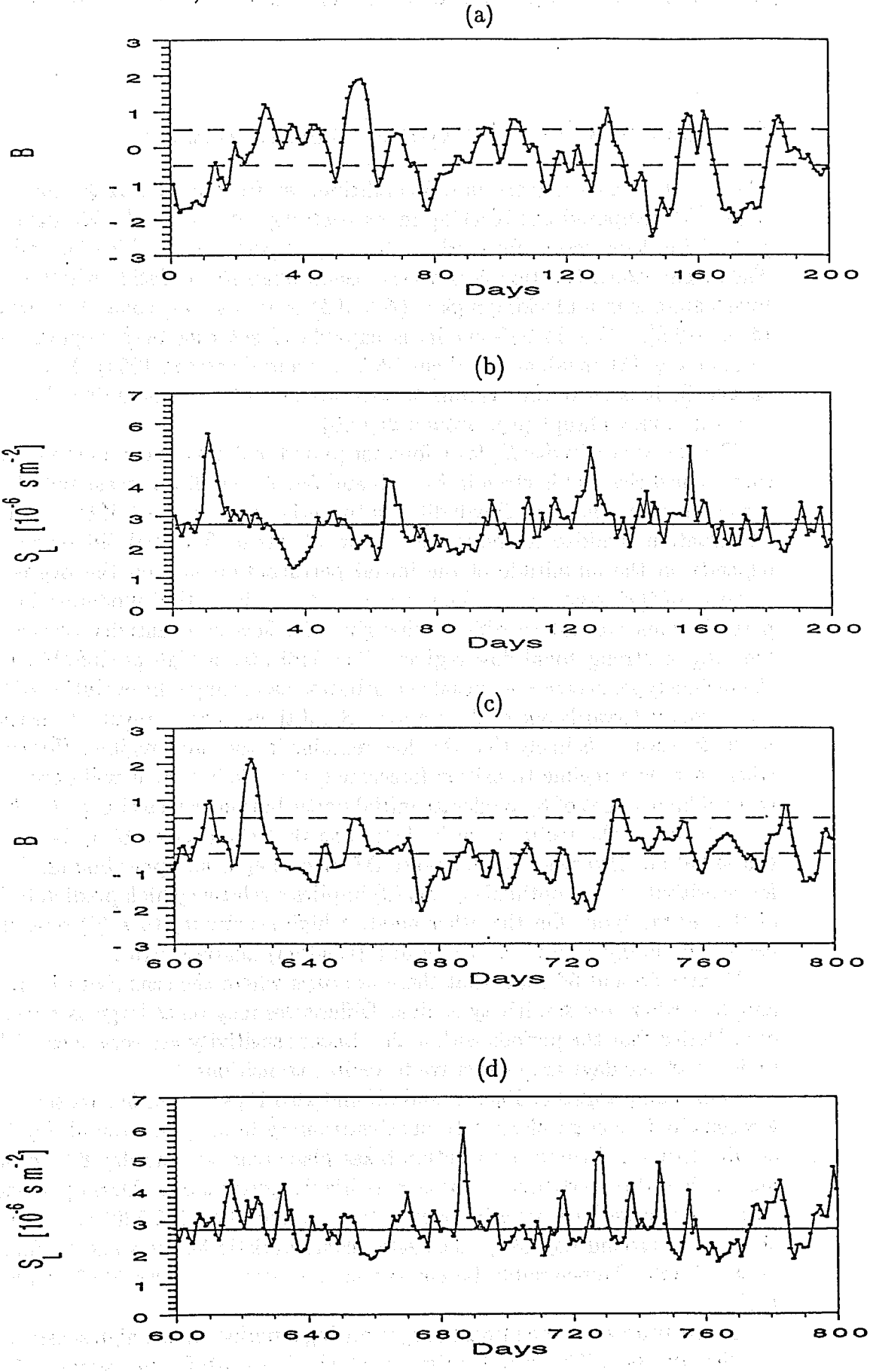

Fig. 5. (a) $\mathcal{B}$ in the period 1 to 200. (b) Linear sensitivity S_L for a forecast period of 3 days during the same period. (c) $\mathcal{B}$ and (d) S_L in the period 600 to 800.

690 is added to the reference field at day 687. The scaling factor λ, see Eq. (15), is chosen in such a way that the error in the geopotential height of the 500 hPa level is everywhere smaller than 15 m. The reference field and the perturbed field are integrated with the nonlinear T21QG model for a forecast period of four days. The evolution of these fields and of the error growth are given in Fig. 6 for the 500 hPa-level. The reference field (Fig. 6b) and perturbed field (Fig. 6c) at day 687 are both zonal above the Atlantic Ocean and Western Europe: for both fields $\mathcal{B}$ = -0.49. The initial optimal perturbation, as is shown in Fig. 6a, is mainly located above North America with its energy distribution concentrated in the smaller scales and has a baroclinic structure (200 hPa and 800 hPa levels are not shown in the Figures). Within one day the perturbation energy is transferred to lower wave numbers (i.e. the larger scales are more pronounced) and the error pattern reveals an equivalent barotropic dipole-like structure. The flow in the western part of the Atlantic Ocean becomes more meridional in the perturbed run. In the consecutive days the error grows very fast and is advected to the east (Fig. 6d). The difference $\Delta\mathcal{B}$ between the perturbed and reference field after three days (optimization time) is 2.02 and the transition to a blocked flow in the perturbed run is clearly visible ($\mathcal{B}$ = 1.78), see (Fig. 6f). After four days $\Delta\mathcal{B}$ is even 2.52, the reference field is in the strong zonal flow regime ($\mathcal{B}$ = -0.63) and the perturbed field in the blocking regime ($\mathcal{B}$ = 1.89).

6 Extension to the nonlinear range

The operational predictability of blocking was studied by Tibaldi and Molteni (1990). They have investigated the ability of the ECMWF Model to represent Euro-Atlantic and Pacific blocking onset and maintenance. It was found that blocking frequency and duration were underestimated in medium-range forecasts. New versions of the model have now been improved. Furthermore, it appeared that when the initial conditions were already blocked, the duration was reasonably well predicted. Very short-range forecasts of blocking onset are fairly successful but the onset is frequently missed beyond day 3 to 4. The inability of predicting blocking onset in the medium-range still has a substantial impact on the systematic model error. As a result of this inability, it is relevant to study the sensitivity of regime transitions to initial conditions beyond day 3. However, by then the evolution of analysis errors can not be considered linear anymore (Lacarra and Talagrand 1988; Vukićević 1991; Errico et al. 1993). As a consequence, the problem arises that the error growth can not be described with a tangent linear model. Therefore, it is proposed to modify the technique as outlined in section 4 for the nonlinear-range.

The modification is based on the following idea. If we add a perturbation with a realistic amplitude to the initial conditions, the error growth is, on av-

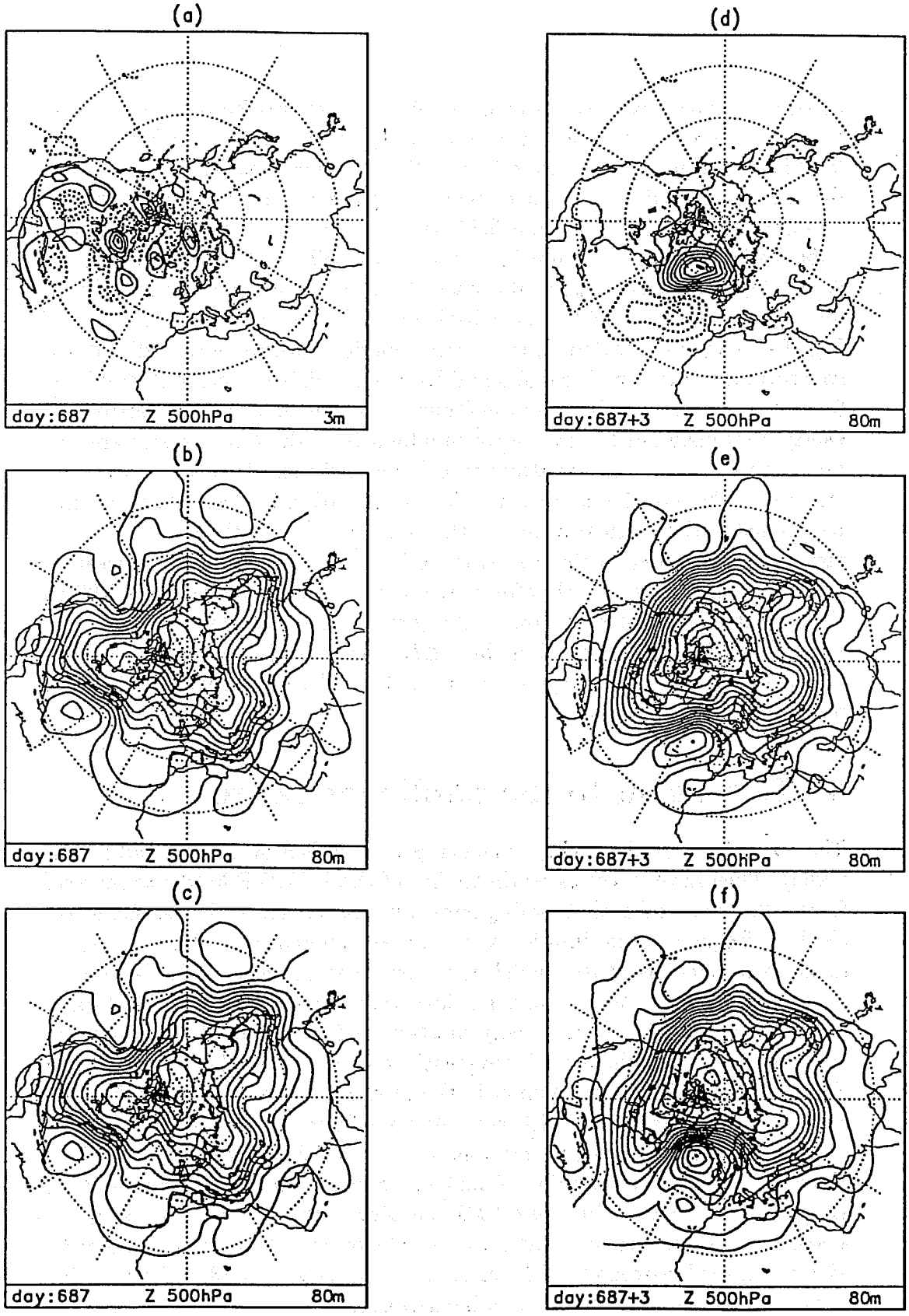

Fig. 6. Geopotential height field at 500 hPa of (a) initial optimal perturbation $\epsilon_L(0)$ for day 687 with optimization time of 3 days, (b) the reference orbit at day 687 and (c) the perturbed orbit at day 687. Nonlinear integration for 3 days of (a), (b) and (c) results in (d), (e) and (f) respectively. Contour intervals are given in each panel.

erage, linear up to day 2 or 3. However, if we add a much smaller perturbation this period will be longer. The amplitude of the initial perturbation and the growth rate determine the length of the linear range. In a finite dimensional model this range can always be extended by decreasing the amplitude of the initial perturbation. On the other hand, in the real atmosphere, an infinite dimensional system, infinitesimal perturbations may evolve into large perturbations in a finite time. It follows that although in the model context the optimization time can be made very large, the modification only makes sense for a maximum optimization time between one and two weeks.

The modification of ϵ_L is achieved by applying an iterative procedure. We start the modification by adding a perturbation $\epsilon_0(0)$, which lies in the direction of ϵ_L, to the reference orbit ψ_0. The amplitude of $\epsilon_0(0)$ must be taken such that its error growth is linear during a period of time T ($T < 10$ days). A new reference orbit ψ_1 is obtained by performing a nonlinear integration with T21QG starting from $\psi_0(0) + \epsilon_0(0)$. Iteratively we now determine $\epsilon_i(0)$, keeping $< \epsilon_i(0), \epsilon_i(0) >$ fixed, so that

$$\mathcal{B}(\psi_i(T) + \epsilon_i(T)) - \mathcal{B}(\psi_0(T)) \tag{18}$$

is maximal or minimal, corresponding to a maximum change towards the blocking regime or strong zonal flow regime, respectively. In this, we assume that the evolution of $\epsilon_i(0)$ is linear with respect to ψ_i for time T. After each iteration, a new reference orbit ψ_{i+1} is determined by starting a model integration from $\psi_i(0) + \epsilon_i(0)$. Because we only need to maximize the difference between two scalar quantities, it is easy to derive that $\epsilon_i(0)$ can also be obtained by maximizing or minimizing the expression

$$\mathcal{B}(\psi_i(T) + \epsilon_i(T)) - \mathcal{B}(\psi_i(T)) \ . \tag{19}$$

Thus, the computation of $\epsilon_i(0)$ is reduced to the determination of ϵ_L with respect to ψ_i, which is described in section 4. The iterative procedure ends when the sum of the perturbations

$$\epsilon_{NL}(0) = \sum_{i=0}^{N} (\epsilon_L(0))_i \tag{20}$$

has the same norm as the original linearly optimal perturbation. In the linear case, the perturbation which is optimal for inducing a blocking regime differs only in sign from the one which optimally induces a strong zonal flow regime. However, in the nonlinear case the perturbations, obtained by either maximizing or minimizing each step (19), have different structures after at least two steps. Namely, after adding or subtracting $\epsilon_1(0)$ to the reference flow two different new reference orbits will be obtained, so that the maximization and minimization procedures are not symmetric anymore. The procedure does not

guarantee that of all perturbations with this norm, ϵ_{NL} results in the maximum difference in $\mathcal{B}$ because the iterative algorithm can also lead to a local maximum. However, as we will see, the procedure works well in the sense that when ϵ_{NL} is added to the initial stream function $\psi(0)$, $\Delta\mathcal{B}$ is substantially larger than obtained with ϵ_L when the nonlinear-range is entered.

In this way, we can still use the linear adjoint operator R^* in each iteration but are able to extend the method into the nonlinear range. The same procedure is described in Barkmeijer (1995). Maximizing the cost function $\Delta\mathcal{B}$ iteratively is related to the iterative minimization procedures used in the context of four-dimensional data assimilation, see Thépaut et al. (1991) and Zupanski (1993).

In Fig. 7 results are given for an optimization time T of 6 days (144h) for all days between days 701 and 800. This period is chosen because of the high variability in the linear sensitivity S_L (see Fig. 5d). The difference in $\mathcal{B}$ of the perturbed flow towards a blocking regime is computed in three ways. The dashed line gives $\Delta\mathcal{B}$ when the perturbation ϵ_L is added to the reference flow and error growth would be purely linear. The perturbation ϵ_L has every day the same initial amplitude such that the maximum value is about 15 m at 500 hPa. One way to compute $\Delta\mathcal{B}$ is to integrate ϵ_L with the tangent linear operator R, but it can also be calculated directly using equation (16). The dotted line gives for the same perturbation ϵ_L the results for the nonlinear integrations. Comparing these two lines, one can see that in general the linear theory overestimates the error growth for ϵ_L. The solid line gives $\Delta\mathcal{B}$ when ϵ_{NL} with the same length as ϵ_L is added to the initial conditions and integrated in time with the nonlinear model. The number of iterations used varies between 5 and 7. It appeared that the iterative procedure is not very sensitive to the size of the amplitude of the optimal perturbation that is computed in each iteration. Comparing the results of the nonlinear integrations with the orbits perturbed with ϵ_L and ϵ_{NL} one can conclude that modification of the initial error pattern ϵ_L can compensate for the saturation of the error growth due to nonlinear interactions.

We point out that the dashed line and solid line are correlated ($\rho = 0.76$). It seems that linear theory still enables one to determine if a circulation pattern is sensitive to small changes in the initial conditions or not, although nonlinear error growth is non-negligible. So, S_L still might provide an efficient predictor for possible transitions. If one is interested in the fastest-growing error patterns, the computation of ϵ_{NL} is needed.

An example which clearly illustrates the impact of the modification procedure is shown in Figs 8 and 9. In Fig. 8, the evolutions of ϵ_L and ϵ_{NL} are compared. The reference forecast orbit starts from day 722 and the optimization time T is 6 days. Both perturbations ϵ_L and ϵ_{NL} have initially the same length and their geopotential height fields at 500 hPa are given in Figs 8a and 8b respectively. In computing ϵ_{NL} we used 7 iterations. The main part of

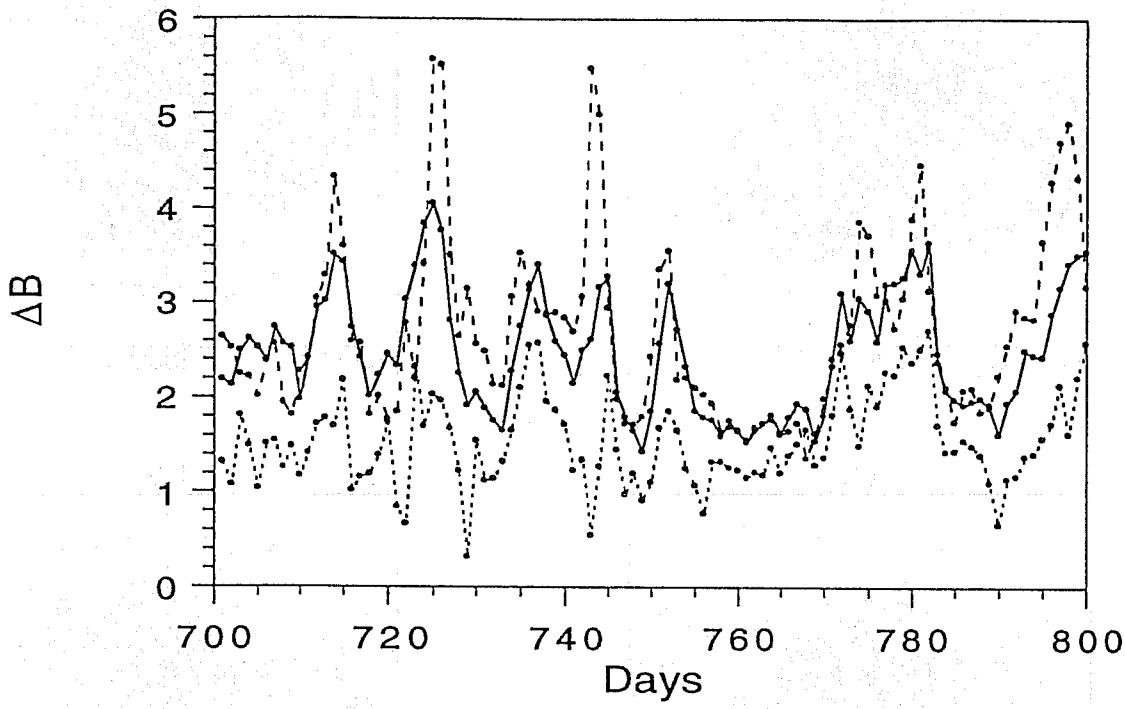

Fig. 7. The difference $\Delta\mathcal{B}$ when the optimal perturbation is added to the reference field with an optimization time T of 6 days for all days in the period 701 to 800. The dashed line corresponds with a linear integration of ϵ_L and a nonlinear integration of ϵ_L is given by a dotted line. The solid line shows $\Delta\mathcal{B}$ when ϵ_{NL} is nonlinearly integrated.

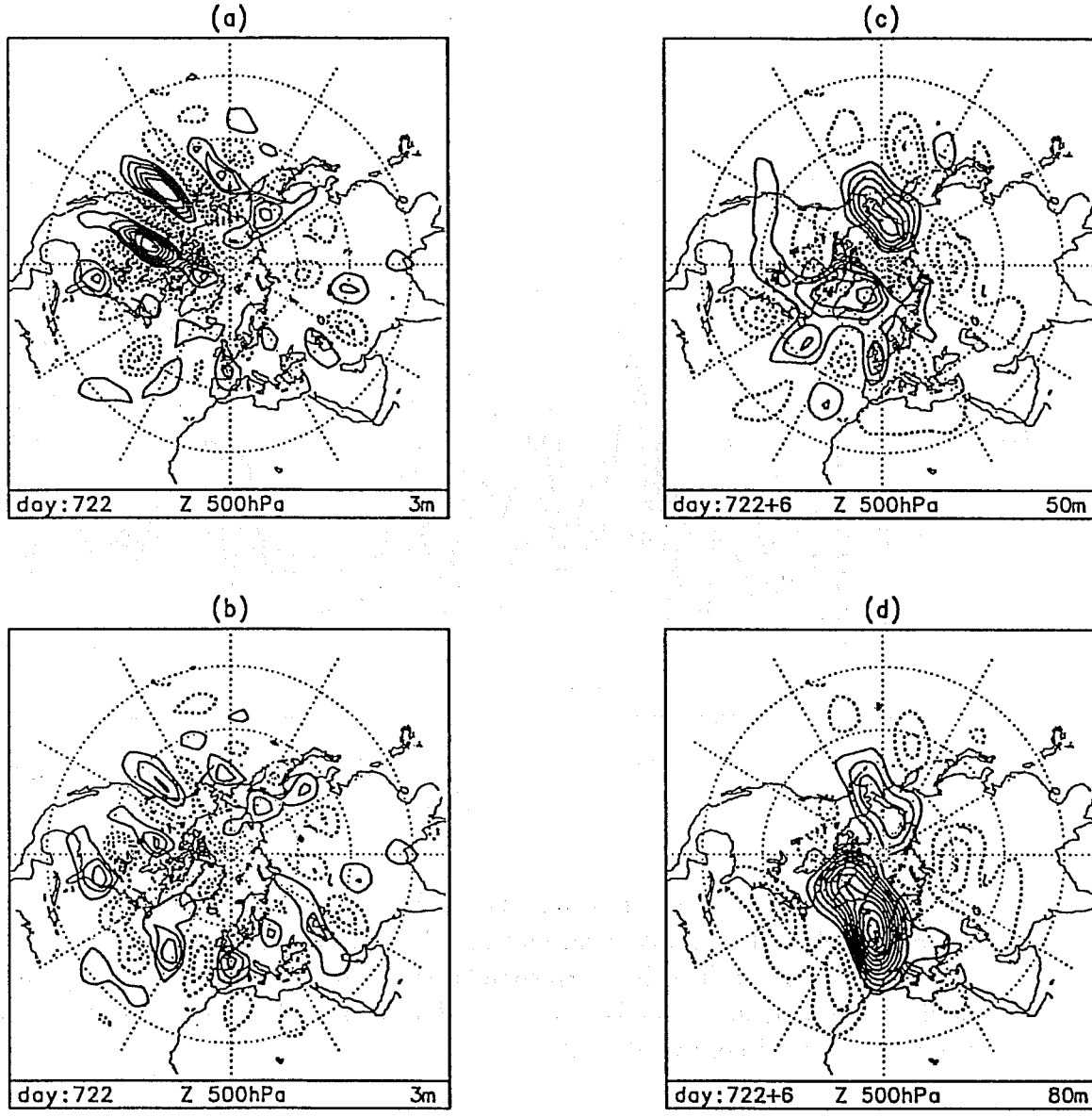

Fig. 8. Geopotential height field of the initial optimal perturbations (a) ϵ_L and (b) ϵ_{NL} at 500 hPa for day 722 with optimization time of 6 days. Final errors (c) ϵ_L and (d) ϵ_{NL} after 6 days. Contour intervals are given in each panel.

ϵ_L is located in the North American area, whereas ϵ_{NL} has a more global nature. The nonlinear modification of ϵ_{NL} mainly affects the strength of the local structures, not the position. After two days the initially small-scale, baroclinic structures have evolved into larger scale and equivalent barotropic structures. The error growth of ϵ_L is faster than ϵ_{NL} during the first four days, which can be expected, but decreases after day five. At optimization time, ϵ_L has only a small amplitude over the Atlantic and Western European areas (Fig. 8c). The modified perturbation ϵ_{NL} continues to grow in the nonlinear-range and shows a large projection onto the blocking anomaly pattern at optimization time (Fig. 8d). Figure 9 gives the geopotential height patterns at optimization time of the reference orbit (Fig. 9a), the orbit perturbed with ϵ_L (Fig. 9b) and ϵ_{NL} (Fig. 9c). The perturbation ϵ_L was not able to initiate a transition. Both Figs 9a and 9b are in the strong zonal flow regime with $\mathcal{B}$ values of -2.1 and -1.4 respectively. Figure 9c indicates that a transition to a blocked flow is possible at day 6 ($\mathcal{B}$= 0.86) by using ϵ_{NL} as initial perturbation.

In Fig. 10, $\Delta\mathcal{B}$ at forecast day 6 computed with T21QG for all days between days 701 and 800, shown in Fig. 7, is added to $\mathcal{B}$ of the reference flow. It turns out that 74 days perturbed with ϵ_L and 94 days perturbed with ϵ_{NL} are blocked ($\mathcal{B} > 0.5$). This means that almost always a block can develop within six days. In the same way, we have tried to decrease $\mathcal{B}$ every day to get a strong zonal flow. We have found the same high rates of transitions to this regime (not presented). Of course, the probability of such a development is important. Results show that by adding ϵ_{NL} to the reference flow, the model is forced into regions on the attractor which it rarely visits. In almost 50% of all cases $\mathcal{B}$ becomes larger than 2, a value which is exceeded only a few times in the 1000-day dataset (Figs 5a and 5c). From this, it can be concluded that the optimal error is very special. Probably, an analysis error usually has a low projection on it.

7 Concluding remarks

In the first part of this paper the KNMI ensemble prediction system (KEPS) is presented. The method is based on the assumption of linear error growth. It uses adjoint models and is applied for the short term only. This scheme is now entering its operational phase.

In the second part we have studied the sensitivity to initial conditions of the onset of blocking and strong zonal flow regimes in the Atlantic-European area. For short optimization times and perturbations with realistic amplitudes, error growth is almost linear. The sensitivity varies from day to day with only short periods of a high sensitivity. Results show that during these short periods, perturbations may initiate a regime transition. It might be useful to investigate the periods with high sensitivity in order to obtain some insight in

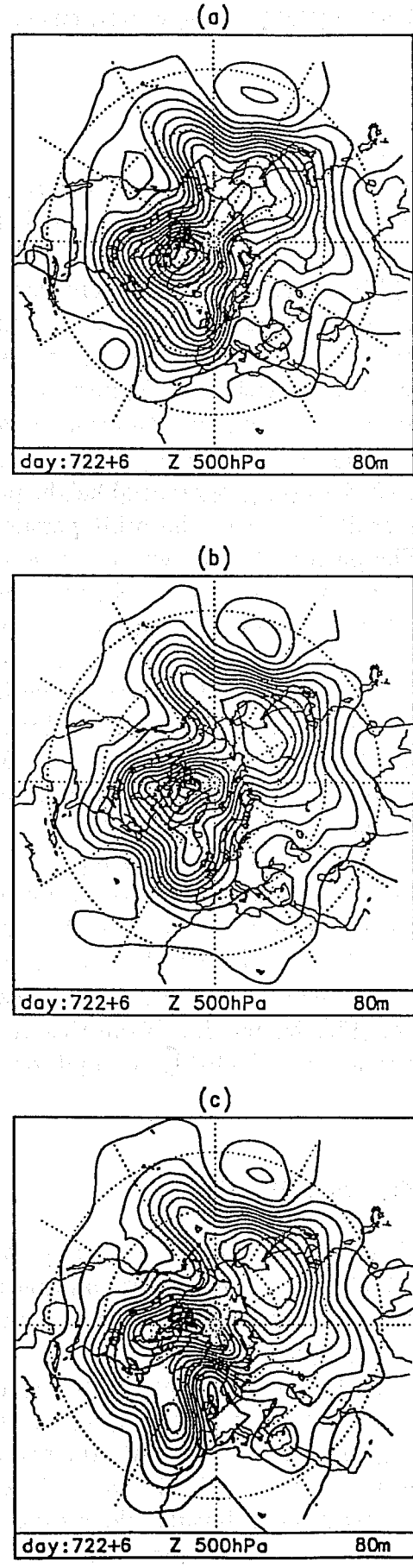

Fig. 9. Geopotential height patterns at optimization time (6 days) of (a) reference orbit and the reference orbit perturbed with (b) ϵ_L and (c) ϵ_{NL} after nonlinear integration. Contour interval is 80 m.

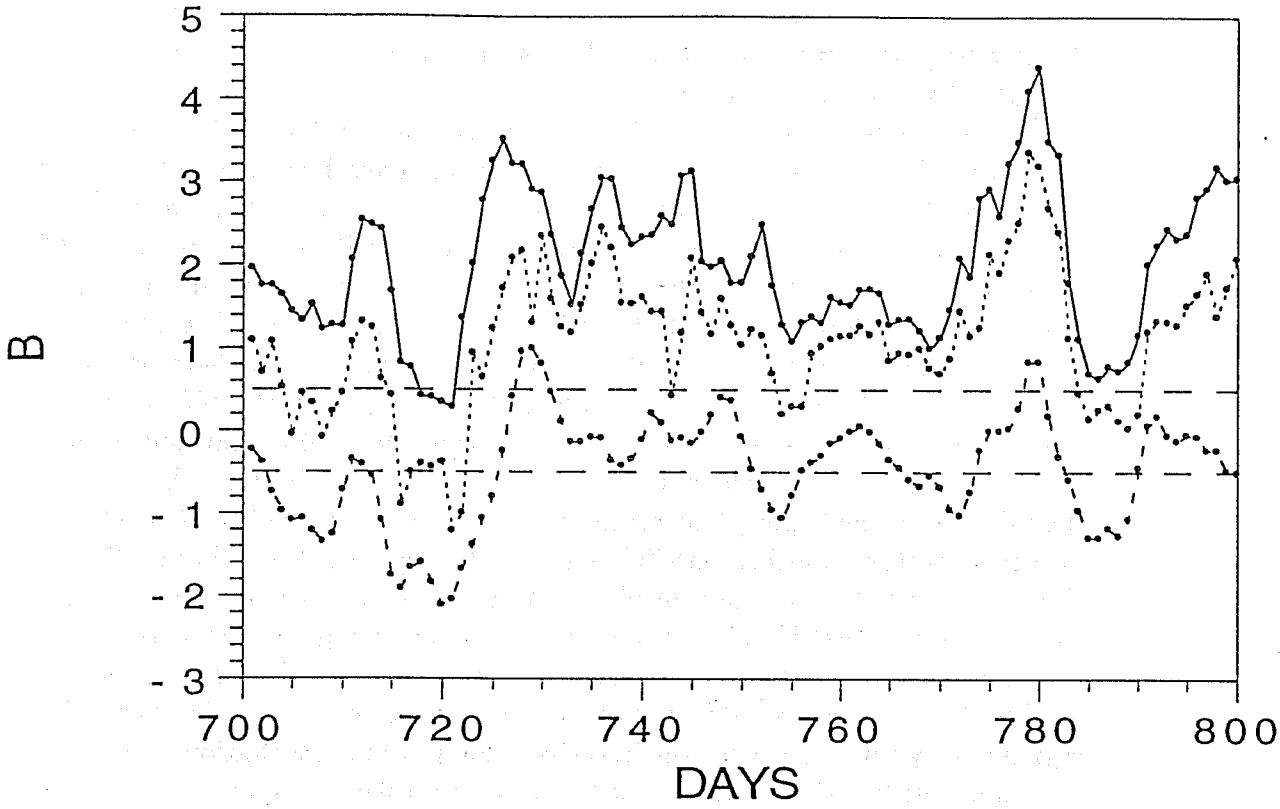

Fig. 10. $\mathcal{B}$ in the period 701 to 800 for the reference flow (dashed line) and the flows perturbed with ϵ_L (dotted line) and ϵ_{NL} (solid line) all nonlinearly integrated.

the mechanisms which play a role in triggering a blocking onset or breakdown. For an optimization time of two or three days, the perturbations mainly originate from North America and are subsequently advected to the east. Thus, features of the jet stream like its strength, geographical position and diffluent character are likely to be important. The sensitive periods may show some general properties which could possibly be revealed in this way. These issues will be made part of future studies.

For longer optimization times error growth is affected by nonlinear interactions. For the medium-range, perturbations have been computed which maximize the difference in $\mathcal{B}$ using an iterative procedure. Experiments have been performed for an optimization time of 6 days with a time series of 100 days. For each day, the optimal perturbation was computed. It was found that almost all these perturbations (with realistic initial length) were able to trigger a blocking regime or a strong zonal flow regime. Furthermore, very large values of $\mathcal{B}$ could be obtained, which did not occur in the 1000 days reference orbit. So, it seems that these perturbations can induce extreme events. The special character of the perturbations can be caused because they do not lie, initially, in the hyper plane given by the local directions of the trajectories on the attractor. Another possibility is that the optimal perturbation lies on the attractor but in a region in phase space, given by all points that trigger extreme events, that is only a small part of the error region around the reference point. In the latter case a transition could be possible, but is still very unlikely because the probability that the initial condition lies in this particular region is very small. Because the iteratively computed perturbations maximize the same cost function as the linearly optimal perturbations, one may assume that there is no substantial difference between them. In turn, the linearly optimal perturbations are strongly related to the fastest-growing singular vectors, sothat the special character could hold for the latter ones too. This is consistent with the results of Anderson (1995), who found that in the three-variable Lorenz convective model the fastest-growing singular vectors do not lie in the local tangent plane to the attractor.

Our approach of constructing perturbations, conceivably with additional constraints concerning above remarks, could be useful for ensemble forecasting. In the ensemble forecasting technique, a set of slightly different initial states is integrated in time (Lorenz 1965; Leith 1974). The divergence of the trajectories is taken as a measure of the predictability. In this way, the skill of the operational numerical weather prediction (NWP) models could be estimated in advance. It is, however, difficult to define a set of initial states which is not too large and at the same time gives statistically representative information about the divergence of the flow. Current methods to compute a set of initial states are making use of singular vectors (Mureau et al. 1993; Buizza et al. 1993) or bred perturbations (Toth and Kalnay 1993). Results of these methods show that the spread in the medium-range is usually too

small (ECMWF 1993). The iterative algorithm presented in this paper can be useful to compose an ensemble which produces a significantly larger spread in the nonlinear-range.

Moreover, one of the main objectives of ensemble forecasting is to detect possible regime transitions which are not forecasted by a general circulation model (GCM). The GCM's are in many cases not able to predict regime transitions beyond a few days correctly (Tibaldi and Molteni 1990). An important reason for this inability is that the onset of a regime is usually very sensitive to the initial conditions (as is shown in this paper for a blocking and strong zonal flow regime). An ensemble prediction system (EPS) should warn for a possible regime transition. However, none of the present ensemble prediction systems specifically selects initial perturbations which trigger the onset of a particular weather regime. An alternative set of initial perturbations for an EPS can be computed by a generalization of our method. In the same way as for the blocking anomaly pattern, perturbations can be computed which maximize the projection onto the anomaly patterns of other regimes or flow patterns. A possible choice of patterns are the first N empirical orthogonal functions (EOF's) which explain most of the variance of the flow. Then, the ensemble of initial perturbations consists of perturbations which maximize the projection on these EOF's at a prescribed forecast time.

Our results for the medium-range indicated that a large spread could be produced for almost every initial condition. When such large spreads can be produced in more realistic models, one must doubt the usefulness of a predictability estimate obtained with a small ensemble. By this we mean that almost all weather scenarios (i.e. Großwetterlage patterns) may occur in the medium-range for initial perturbations comparable to current analysis errors.

Acknowledgements. Many thanks are due to the members of the predictability section at KNMI for the stimulating discussions and their assistance during the preparation of this paper. This work has been supported by the foundation for Geological, Oceanografic and Atmospheric Research (GOA) of the Netherlands Organisation for Scientific Research (NWO). Computing facilities are provided by the Royal Netherlands Meteorological Institute.

8 References

Anderson, J.L., 1995: Selection of Initial Conditions for Ensemble Forecasts in a Simple Perfect Model Framework. *J. Atmos. Sci., In press.*

Barkmeijer, J. 1992: Local error growth in a barotropic model. *Tellus*, **44A**, 314-323.

Barkmeijer, J. and J.D. Opsteegh, 1992: Local skill predictions for the ECMWF model using adjoint techniques. In *New developments in predictability* Proceedings of ECMWF workshop, 1991, Reading, UK, 55-64.

Barkmeijer, J. 1995: Constructing fast-growing perturbations for the nonlinear regime. *J. Atmos. Sci., In press.*

Buizza, R., J. Tribbia, F. Molteni, and T. Palmer, 1993: Computation of optimal unstable structures for a numerical weather prediction model. *Tellus*, **45A**, 388-407.

Dole, R.M. 1978: The objective representation of blocking patterns. In *The general circulation: theory, modeling and observations.* Notes from a Colloquium, Summer, 1978. NCAR/CQ - 6 + 1978 - ASP, 406 - 426.

ECMWF, 1993: *Expert meeting on ensemble prediction system 6-7 July 1993.* Report of expert meeting. Reading, England, ECMWF, 133 pp.

Errico, R.M., T. Vukićević, 1992: Sensitivity analysis using the adjoint of the PSU/NCAR mesoscale model. *Mon. Wea. Rev.*, **120**, 1644-1660.

Errico, R.M., T. Vukićević, and K. Reader, 1993: Examination of the accuracy of a tangent linear model. *Tellus*, **45A**, 462-477.

Farrell, B. 1989: Optimal excitation of baroclinic waves. *J.Atmos. Sci.*, **46**, 1193-1206.

Lacarra, J. and O. Talagrand, 1988: Short-range evolution of small perturbations in a barotropic model. *Tellus*, **40A**, 81-95.

Leith, C.E. 1974: Theoretical Skill of Monte Carlo Forecasts. *Mon. Wea. Rev.*, **102**, 409-418.

Liu, Q. 1994: On the definition and persistence of blocking. *Tellus*, **46A**, 286-298.

——, and J.D. Opsteegh, 1994: Inter annual and decadal variations of blocking activity in a quasi-geostrophic model. *Tellus, In press.*

Lorenz, E.N. 1963: Deterministic Nonperiodic Flow. *J. Atmos. Sci.*, **20**, 130-141.

——, 1965: A study of the predictability of a 28-variable atmospheric model.

Tellus, **17**, 321-333.

Marchuk,G.I. 1974: Numerical solution of the problems of the dynamics of the atmosphere and the ocean. Academic Press New York, 387 pp.

Marshall, J. and F. Molteni, 1993: Toward a Dynamical Understanding of Planetary-scale Flow Regimes. *J. Atmos. Sci.*, **50**, 1792-1818.

Molteni, F., and T.N. Palmer, 1993: Predictability and finite-time instability of the northern winter circulation. *Q. J. R. Meteorol. Soc.*, **119**, 269-298.

Mureau, R., F. Molteni, and T.N. Palmer, 1993. Ensemble predictions using dynamically-conditioned perturbations. *Q. J. R. Meteor. Soc.*, **119**, 299-323.

Palmer, T.N., Č. Branković, , F. Molteni, and S. Tibaldi, 1990: Extended-range predictions with ECMWF models: Interannual variability in operational model integrations. *Q. J. R. Meteor. Soc.*, **116**, 799-834.

——, 1993: Extended-range atmospheric prediction and the Lorenz model. *Bulletin of the American Meteorological Society*, **74**, 49-65.

Rex, D.F. 1950a: Blocking action in the middle troposphere and its effect upon regional climate. I. An aerological study of blocking. *Tellus*, **2**, 196-211.

——, 1950b: Blocking action in the middle troposphere and its effect upon regional climate. II. An aerological study of blocking. *Tellus*, **2**, 275-301.

Talagrand, O. and P. Courtier, 1987: Variational assimilation of meteorological observations with the adjoint vorticity equation. I: Theory. *Q. J. R. Meteorol. Soc.*, **113**, 1311-1328.

Thépaut, J.N., and P. Courtier, 1991: Four dimensional variational data assimilation using the adjoint of a multilevel primitive equation model. *Q. J. R. Meteor. Soc.*, **117**, 1225-1254.

Tibaldi, S. and F. Molteni, 1990: On the operational predictability of blocking. *Tellus*, **42A**, 343-365.

Toth., Z. and E. Kalnay, 1993: Ensemble forecasting at NMC: The generation of perturbations. *Bull. Amer. Meteor. Soc.*, **74**, 2317-2330.

Vautard, R. 1990: Multiple Weather Regimes over the North Atlantic: Analysis of Precursors and Successors. *Mon. Wea. Rev.*, **118**, 2056-2081.

Vukićević, T. 1991: Nonlinear and linear evolution of initial forecast errors. *Mon. Wea. Rev.*, **119**, 1602-1611.

Zhang, Z. 1988: The linear study of zonally asymmetric barotropic flows. PhD thesis, University Reading, UK, 163pp.

Zupanski, M., 1993: Regional Four-Dimensional Variational Data Assimilation in a Quasi-Operational Forecasting Environment. *Mon. Wea. Rev.*, **121**, 2396-2408.